Volume 1 | Number 1 | Jan 2013 | Pages 1–100

**PCCP**

Physical Chemistry Chemical Physics
www.rsc.org/pccp

ROYAL SOCIETY OF CHEMISTRY

ROYAL SOCIETY OF CHEMISTRY

www.rsc.org/pccp

# PCCP

## ARTICLE

# Viability of Aromatic All-Pnictogen Anions

Subhajit Mandal,[a,b] Surajit Nandi,[b] Anakuthil Anoop*[b] and Pratim Kumar Chattaraj*[a]

Aromaticity in novel cyclic all-pnictogen heterocyclic anions, $P_2N_3^-$, $P_3N_2^-$ and their heavier analogues is studied using quantum mechanical computations. All geometrical parameters from optimized geometry, bonding, electron density analysis from Quantum theory of Atoms in Molecules, Nucleus-Independent Chemical Shift, and Ring Current Density plots, support their aromaticity. The aromatic nature of these molecules closely resembles the prototypical aromatic anion, $C_5H_5^-$. These singlet $C_{2v}$ symmetric molecules are comprised of five distinct cannonical structures and are stable upto atleast 1000 fs without any significant distortion. Mechanic study reveals a plausible synthetic pathway for $P_3N_2^-$ – a click reaction between $N_2$ and $P_3^-$, through a $C_{2v}$ symmetrtic transition state. Beside this, the possibility of $P_3N_2^-$ as a $\eta^5$-ligand in metallocenes is studied and the nature of bonding in the metallocenes are discussed through the energy decomposition analysis.

## Introduction

Aromaticity is a special feature of planar, cyclic structures with delocalized $(4n+2)-\pi$ electrons, that gives rise to extra stability compared to their acyclic analogues. After recognition of benzene $(C_6H_6)$ as the classical example of aromatic molecule by Kekulé,[1] several studies have been carried out to characterize and quantify the aromaticity in hydrocarbons, mostly through *in silico* experiments.[2] Even now, detection of aromaticity in non-carbocyclic compounds containing all-metals[3] or all-main-group elements sparks enormous interest among chemists. Among the main group aromatics, pnictogen heterocycles are important due to their resemblance with aromatic carbocycles and utility as high energy density material (HEDM).[4]

Attempts for the experimental realization and theoretical characterization and prediction of all-pnictogen aromatic compounds are in progress for the last four decades. The lightest homocyclic all-pnictogen aromatic compound, pentaazolate ion $(N_5^-)$, is characterized theoretically[5] as a planar, $6\pi$ electron system. Although, it resembles cyclopentadienide ion $(C_5H_5^-)$, $N_5^-$ has been observed only in tandem mass spectroscopy as a gas-phase ion where $N_5^-$ gets dissociated to $N_3^-$ and $N_2$.[5a] The cation, $N_5^+$ is acyclic because

cyclic geometry is antiaromatic (having $4\pi$ electrons).[6] Cyclic hexazine $(N_6)$, the benzene analogue, was thought to be prepared experimentally,[7a] however, its existence is debated[7b-d] mainly because of high endothermic formation energy. All-phosphorous homocycle, pentaphosphacyclopentadienide ion $(P_5^-)$, was isolated as $NaP_5$ solution which remains stable for 7–10 days in room temperature under anaerobic condition.[8a] Theoretical study[8b-c] suggests $P_5^-$ as a planar, $6\pi$–electron aromatic. Moreover, it can substitute $C_5Me_5$ in ferrocene-like complexes.[8d] The all-phosphorus benzene-analogue, $P_6$,[9] is characterized theoretically, yet to be synthesized.
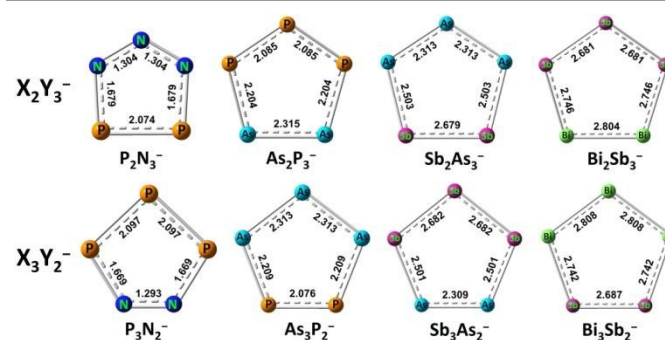


**Fig. 1** Optimized singlet state $C_{2v}$ symmetric geometries of $X_2Y_3^-$ and $X_3Y_2^-$ molecules. Distances are in Å units.

Among the molecules made of N and P, the smallest one, PN, is a high energy molecule found in outer space.[10a-b] The $N_2P^-$, $NP_2^-$ and $P_3N_3$, are also studied theoretically.[10c-d] The latest one is the cyclic $P_2N_3^-$, synthesized by treating azide $(N_3^-)$ with $P_2(C_{14}H_{10})_2$ in tetrahydrofuran solution,[11] characterized theoretically as a cyclic planar system, containing $6\pi$ electrons, and shows aromaticity resembling $C_5H_5^-$.

Prompted by this report on the synthesis of $P_2N_3^-$, we became interested in a closely related system, $P_3N_2^-$. We have validated its

a. *Department of Chemistry and Centre for Theoretical Studies,*
   *Indian Institute of Technology Kharagpur, Kharagpur 721302, India.*
   *Email: pkc@chem.iitkgp.ernet.in.*
b. *Department of Chemistry,*
   *Indian Institute of Technology Kharagpur, Kharagpur 721302, India.*
   *Email: anoop@chem.iitkgp.ernet.in.*

This journal is © The Royal Society of Chemistry 20xx

*Phys. Chem. Chem. Phys.*, 2015, **00**, 1-8 | **1**

aromaticity using geometrical parameters, bonding, and the popular aromaticity indices and propose a potential synthetic route using computational chemistry methods. In addition, we have investigated other five-membered cyclic anions of heavier elements from the same group. We chose two kinds of anions for the computational study: $X_2Y_3^-$ and $X_3Y_2^-$ (Fig. 1) where X is a group 15 element, *viz.* P, As, Sb and Bi, and Y is the immediate lighter element in the same group (N, P, As, and Sb). These cyclic structures are of the type *cyclo–*XXYYY or *cyclo–*XXXYY. These molecules were chosen for this study as they are expected to be more aromatic and stable, among the numerous molecules that are possible from the combination of all pnictogen atoms. In this report, we discuss the structure, stability, aromaticity, potential synthetic route, and their use as ligands.

## Computational Details

All the optimizations of singlet and triplet state geometries are performed in gas phase with Gaussian 09 program package.[12] The Minnesota functional, M06-2X[13] is used for all the optimizations along with def2-TZVPPD[14] basis set. For the heavier atoms, antimony (Sb) and bismuth (Bi), the corresponding pseudopotentials (def2-ecp)[15] are taken into account. The nature of the stationary points is characterized by vibrational frequency calculation – the number of imaginary frequency is zero for substrates, products and intermediates, and is one for transition states. Thermochemical values are calculated at 298 K. Computed electronic energies (E) are corrected for zero-point energy (ZPE). Intrinsic reaction coordinate (IRC) calculations are performed in order to verify that the transition state is connected with both the reactant and product side.

Quantum Theory of Atoms In Molecules (QTAIM)[16a] analysis is performed with Multiwfn software (version 3.3.1)[17] using the wave functions (.wfn) generated at M06-2X/WTBS[18a-b] level of theory with the optimized geometries at M06-2X/def2-TZVPPD level of theory in Gaussian 09. The WTBS is an all electron basis set and therefore the AIM analysis is free from ECP data.[18c] Natural Bond Orbital (NBO)[19] analysis is performed with NBO 5.9 software package.[20] The natural charges on atoms and Wiberg Bond Indices (WBI)[21] are calculated with Natural Population Analysis (NPA). Number of resonance structures and their contributions are calculated with Natural Resonance Theory (NRT)[19b] as implemented in NBO 5.9.

Ring Current Density plots are generated with AIMAll software package (version 15.05.18).[22] Single point computations are done at M06-2X/def2-SVP[23] level of theory on the previously optimized geometries (at M06-2X/def2-TZVPPD level). The .wfx and .fchk files are generated from NMR calculations by the Gaussian 09 using the GIAO[24] method.

*Ab initio* molecular dynamics simulation is carried out using the Atom-centered Density Matrix Propagation (ADMP)[25] technique as implemented in Gaussian 09 at the M06-2X/def2-TZVPP[23b,26] level. Boltzmann distribution was used for generating the initial nuclear kinetic energies of the systems. The temperature was maintained through a velocity scaling thermostat throughout the simulation. For each of the systems, a simulation was carried out separately at 298 K and at 400 K. A default random number generator seed was used, as implemented in Gaussian 09, to initiate the initial mass weighted Cartesian velocity. For each case, the trajectories were generated for up to 1000 fs.

The optimizations of metallocenes are performed at M06-L[27]/def2-TZVP[26] level in Gaussian 09. For the metal atoms (Fe, Ru, Os) corresponding pseudopotentials[28] are taken into account. Energy decomposition analysis (EDA)[29] is performed with ADF[30] software package at PBE(D3)/TZ2P//M06-L/def2-TZVP level of theory.

## Results and discussion

A rough idea about the relative stabilities of these closely related molecules can be gained from the energy difference between triplet and singlet states ($\Delta E_{T-S}$). The larger $\Delta E_{T-S}$ indicates more relative stability of the molecules in the corresponding singlet state.[31a] Recently synthesized $P_2N_3^-$ has higher $\Delta E_{T-S}$ (65.89 kcal/mol) than the $P_3N_2^-$ (52.18 kcal/mol), and in general all $X_2Y_3^-$ species has higher $\Delta E_{T-S}$ compared to the corresponding $X_3Y_2^-$ species (Table 1). Towards the heavier analogues, the $\Delta E_{T-S}$ decreases. Optimized geometries of all the $X_2Y_3^-$ and $X_3Y_2^-$ species in their singlet state are planar ($C_{2v}$ symmetry) (Fig. 1) – a primary criterion for aromaticity. The triplet state ($^3A$) geometries are non-planar.

**Table 1** Zero point energy (ZPE) corrected relative electronic energy ($\Delta E_{T-S}$) in kcal/mol for the $X_2Y_3^-$ and $X_3Y_2^-$ molecules in their singlet and triplet electronic states, the energy gap between LUMO and HOMO ($E_{L-H}$) in eV, the reactivity descriptors – hardness (η), electronegativity (χ) and electrophilicity (ω) in eV for $X_2Y_3^-$ and $X_3Y_2^-$ molecules in singlet electronic state.

| Molecule | $\Delta E_{T-S}$ (kcal/mol) | $E_{L-H}$ (eV) | η (eV) | χ (eV) | ω (eV) |
|---|---|---|---|---|---|
| $P_2N_3^-$ | 65.89 | 7.208 | 7.208 | 1.604 | 0.178 |
| $As_2P_3^-$ | 43.94 | 5.652 | 5.652 | 1.583 | 0.222 |
| $Sb_2As_3^-$ | 24.76 | 4.795 | 4.795 | 1.453 | 0.220 |
| $Bi_2Sb_3^-$ | 7.06 | 4.352 | 4.352 | 1.282 | 0.189 |
| $P_3N_2^-$ | 52.18 | 6.570 | 6.570 | 1.519 | 0.175 |
| $As_3P_2^-$ | 41.85 | 5.490 | 5.490 | 1.554 | 0.220 |
| $Sb_3As_2^-$ | 22.91 | 4.628 | 4.628 | 1.427 | 0.220 |
| $Bi_3Sb_2^-$ | 2.08 | 4.303 | 4.303 | 1.233 | 0.177 |

A closely related qualitative indicator for stability is the energy difference between the lowest unoccupied molecular orbital (LUMO) and the highest occupied molecular orbital (HOMO).[31b-c] The gap between LUMO and HOMO energies ($\Delta E_{L-H}$) decreases on moving from lighter to heavier analogues (Table 1 and see ESI†, Table S2). The $\Delta E_{L-H}$ of $X_2Y_3^-$ is higher than that of the corresponding $X_3Y_2^-$ species. The trend from $\Delta E_{L-H}$ is similar to $\Delta E_{T-S}$, the $X_2Y_3^-$ is more stable than $X_3Y_2^-$ and stability decreases at heavier analogues. For example, $\Delta E_{L-H}$ of $P_2N_3^-$ is 7.208 eV, whereas that of $P_3N_2^-$ is 6.570 eV. This trend can be justified with the reduction in the hardness (η), *vis-à-vis* the maximum hardness principle[32] (Table 1).

The molecular orbitals are similar to those of the five–membered aromatic molecule, $C_5H_5^-$ – three occupied π–molecular orbitals (MO), including an MO where all the *p*–orbitals are delocalized over all the atoms to form a nodeless π–cloud, a characteristic of aromatic compounds. All the occupied π–MOs of

**2** | *Phys. Chem. Chem. Phys.*, 2015, **00**, 1-8

This journal is © The Royal Society of Chemistry 20xx

$P_2N_3^-$ and $P_3N_2^-$ are similar to those of $C_5H_5^-$ (Fig. 2). Each atom of $X_2Y_3^-$ and $X_3Y_2^-$ has a lone pair of electrons in the plane of the ring in addition to the σ and π–electrons, as per Natural bond orbital (NBO)[19a] analysis. The plots of Electron Localization Function (ELF) (Fig. 3) show these lone pair of electrons in the ring-plane. These plots show that the electron localization is higher on lighter atoms than on the heavier atoms. Further, the localization of electron between the bond decreases down the group, indicating less covalency in the X-X, Y-Y and X-Y bonds.
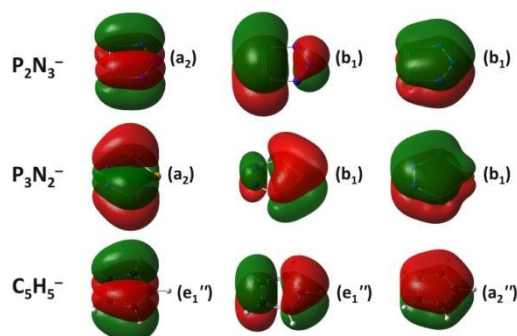


**Fig. 2** Three occupied π–molecular orbitals of $P_2N_3^-$, $P_3N_2^-$ and $C_5H_5^-$. Orbital symmetries are given in the parenthesis.

The canonical bonding situation comprises of five σ–bonds and two conjugated π–bonds. The σ–bonds are made by the overlap of hybrid orbitals – e.g., the N–N σ–bonds in $P_3N_2^-$ and $P_2N_3^-$ are made up of $sp^2$ orbitals. The $p$–character increases in heavier atoms. The lone pair occupies one of these in-plane hybrid orbitals. The two π–bonds are formed by the overlap of two $p$–orbitals of the adjacent atoms. The remaining atom has one $p$–orbital perpendicular to the ring plane which hosts a lone pair of electrons that takes part in resonance. Five canonical structures, with contribution ranging from *ca.* 10–18% (Fig. 4 and see ESI†, Fig. S5), are shown by calculations using Natural Resonance Theory (NRT)[19b] The negative charge (lone pair in the $p$–orbital) is delocalized by these resonating structures. Resonance structures are characteristic of aromaticity.
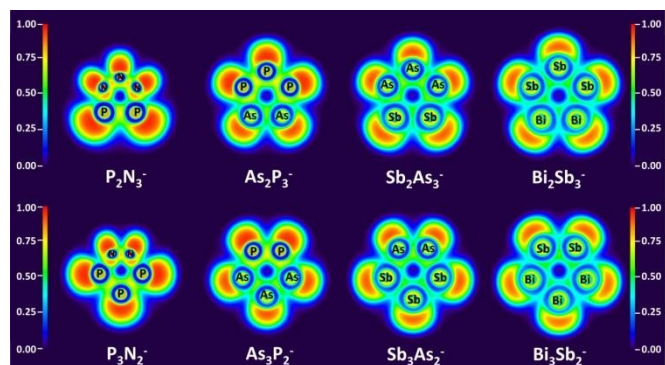


**Fig. 3** Colour filled map of Electron Localization Function (ELF) of $X_2Y_3^-$ and $X_3Y_2^-$ molecules in the molecular plane.

The nature of bonding is analyzed using Quantum Theory of Atoms In Molecules (QTAIM). The Laplacian of the electron density [$\nabla^2\rho(r_c)$] at the (3, -1) bond critical points (BCPs) between X–X, X–Y and Y–Y bonds are negative, i. e. accumulation of electron density, except for N–P, Sb–Bi and Bi–Bi bonds (see ESI†, Table S3a and S3b). Although some of the [$\nabla^2\rho(r_c)$] values are positive, all these bonds show negative $H(r_c)$ which indicates covalent character.[16b] In

addition we have calculated $-G(r_c)/V(r_c)$ because $\nabla^2\rho(r_c)$ alone is not an adequate descriptor for covalent bonding for bonds involving heavier atoms.[16c-d] The bonds with positive $\nabla^2\rho(r_c)$, show [$-G(r_c)/V(r_c)$] value between 0.5 and 1, thus validating covalent bonding in all molecules. All these topological parameters indicate the covalency, which is necessary for aromaticity.
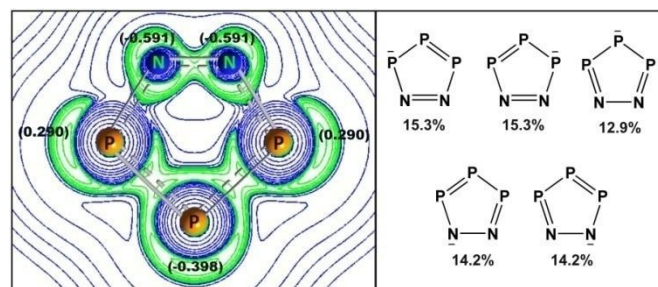


**Fig. 4** Contour plot of the Laplacian of the electron density of $P_3N_2^-$. NPA charges on atoms are shown in parenthesis. The resonance structures are shown with their weightage.

The electron density [$\rho(r_c)$] is not fully delocalized due to the electronegativity differences between the heavier (X) and lighter (Y) atoms. The $\rho(r_c)$ value estimated at the BCPs, is higher in between the lighter atom than in between heavier atoms, as seen in the contour maps of $\nabla^2\rho(r_c)$ (Fig. 4 and see ESI†, Fig. S3a and S3b). The highest value of $\rho(r_c)$ at BCP among the Y-Y bonds is between N–N bond (0.337 a.u.), which decreases successively on going towards heavier elements and reaches lowest value for Bi–Bi bond (0.051 a.u.). This variation in electron density results in the variation in partial charges on the atoms. Natural charges calculated from Natural Population Analysis (NPA)[19c] (see ESI†,Table S4a) show that in both $X_2Y_3^-$ and $X_3Y_2^-$ molecules, lighter atoms (Y) carry more partial negative charges, because electron density is higher in the bonds between lighter atoms.

**Table 2** NICS(0) and NICS(1) values in ppm for the $X_2Y_3^-$ and $X_3Y_2^-$ molecules.

| System | $NICS_{total}(0)$ | $NICS_{zz}(0)$ | $NICS_{total}(1)$ | $NICS_{zz}(1)$ |
|---|---|---|---|---|
| $P_2N_3^-$ | -17.44 | -14.17 | -16.56 | -15.24 |
| $As_2P_3^-$ | -17.19 | -11.58 | -16.55 | -14.48 |
| $Sb_2As_3^-$ | -15.33 | -7.81 | -15.06 | -11.80 |
| $Bi_2Sb_3^-$ | -12.96 | -4.05 | -12.75 | -8.52 |
| $P_3N_2^-$ | -16.85 | -14.12 | -16.51 | -15.29 |
| $As_3P_2^-$ | -17.06 | -10.93 | -16.47 | -14.11 |
| $Sb_3As_2^-$ | -14.69 | -6.89 | -14.49 | -11.01 |
| $Bi_3Sb_2^-$ | -12.71 | -3.64 | -12.43 | -8.09 |

Bond lengths that are in between the single-bond length and double-bond length, and bond orders that are in between 1 and 2 are characteristics of aromaticity. The N-N bond lengths in $P_2N_3^-$ and $P_3N_2^-$ are in between typical N–N distance (1.42 Å)[33a] and N=N distance (1.25 Å)[33b] (Fig. 1). Similarly, all X–X, X–Y and Y–Y. bond lengths in the optimized geometries are less than the sum of their covalent radii.[33] Bond orders from WBI for P–P and N–N bonds are close to 1.5 in $P_3N_2^-$. Similarly, WBI for all the bonds fit into the aforementioned range (see ESI†, Table S4b). The lowest WBI's are found for the P–N bond (1.192 in $P_2N_3^-$ and 1.223 for $P_3N_2^-$).

This journal is © The Royal Society of Chemistry 20xx

*Phys. Chem. Chem. Phys.*, 2015, **00**, 1-8 | **3**

The geometrical and bonding features discussed above are in favor of aromaticity in the planar $X_2Y_3^-$ and $X_3Y_2^-$ molecules. Additional characterization and quantification can be done using popular aromaticity indices such as, Nucleus-Independent Chemical Shift (NICS)[2b]. We have studied a variety of NICS indices to verify the aromaticity of the proposed molecules and also compared the same with the prototypical molecule, $C_5H_5^-$ (Fig. 5). Large negative values of the total chemical shifts ($NICS_{total}$) and the chemical shifts perpendicular to the ring plane ($NICS_{zz}$)[34a] validated the aromatic nature of these molecules (Table 2). The NICS-scan procedure is indicative of both the diamagnetic and paramagnetic ring currents. Therefore, the separation between the in-plane and out-of-plane components of the isotropic NICS is necessary for assigning the diamagnetic and paramagnetic properties for a system. In the NICS-scan approach the nonchemical probe (Bq) atom is placed in the center of the ring and the distance of the probe from the center is increased. The aromaticity decreases on moving down the group due to the increase in the σ−bond length which reduces the overlap between the p−orbitals. The complete $NICS_{total}$−scan (Fig. 5a) and $NICS_{zz}$−scan profiles (Fig. 5b and see ESI†, Fig. S6a) show a minimum at ~ 1 Å above the ring plane, indicating π−aromaticity.
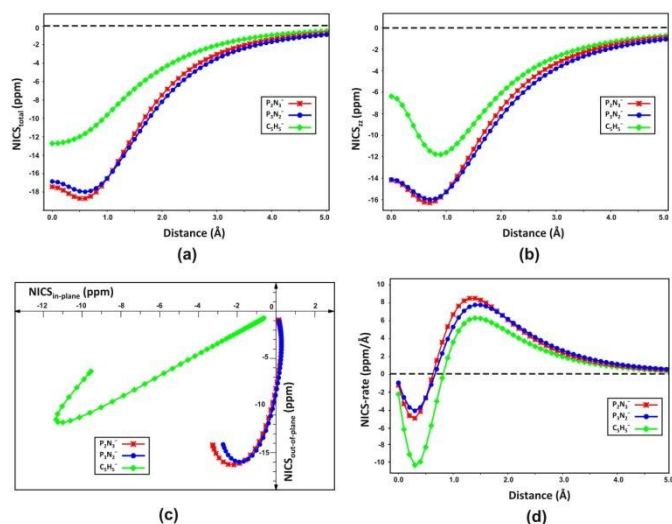


**Fig. 5** NICS plots of $C_5H_5^-$, $P_2N_3^-$ and $P_3N_2^-$. (a) $NICS_{total}$-scan, (b) $NICS_{zz}$-scan, (c) FiPC-NICS-scan, (d) NICS-rate versus r.

The diamagnetic and paramagnetic properties were analyzed individually using Free of in-Plane Component NICS (FiPC–NICS)[34b] scan. Negative $NICS_{out-of-plane}$ with convex slope of the $NICS_{in-plane}$ versus $NICS_{out-of-plane}$ curve ensured aromaticity in $X_2Y_3^-$ and $X_3Y_2^-$ molecules (Fig. 5c and see ESI†, Fig. S6b). The σ− and π−electrons can contribute to the magnetic shielding in aromatic molecules. At the ring centre, the contribution for σ−electrons is significant while π−electrons have more relevance at some distance away from the ring centre. In these molecules, NICS–rate[34c] plots (Fig. 5d and see ESI†, Fig. S6c) along the perpendicular direction of the ring-plane show initial decrease due to the contribution from σ−electrons, followed by an increase owing to π−electrons. In smaller rings, the contribution from π−electrons quickly overcomes the contribution σ−electrons. As the size of the atoms (down the group) increases, contribution of the π−electrons towards the aromaticity reduces,

which can be seen from the late crossing of the NICS−rate plots for the heavier analogues.
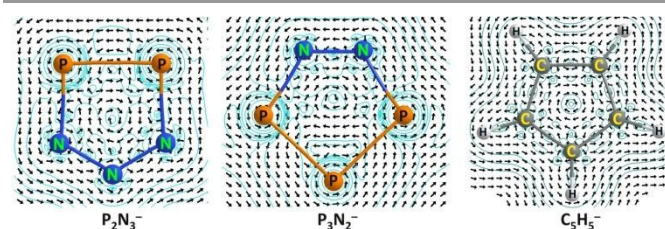


**Fig. 6** Ring Current density maps of $P_2N_3^-$, $P_3N_2^-$ and $C_5H_5^-$.

When an external magnetic field is applied perpendicular to the plane of the molecular ring, it can induce a current density in and parallel to the molecular plane and this current density induces a magnetic field ($\mathbf{B}^{ind}$).[35] Aromatic species are characterized by sustaining diatropic ring current while antiaromatic compounds sustain paratropic ring currents.[2a,d-h] It may be noted that, as the induced magnetic fields and current densities are complementary to each other, they will show similar response while characterizing the aromatic nature in a molecule.[34a] In the same way, $NICS_{zz}$ and the perpendicular to the ring component of the induced magnetic field, ($\mathbf{B}^{ind}_z$) will exhibit similar characteristics.[2e] The current density maps (Fig. 6) in the plane of the ring show circulation of diatropic ring current over the ring frame, and paratropic ring current near the ring centre, which is a feature of aromatic molecules.[36] The circulation of ring currents over the molecular framework (diatropic) as well as in the ring centre (paratropic) for all the $X_2Y_3^-$ and $X_3Y_2^-$ molecules (see ESI†, Fig. S7a and S7b) are similar to that of the prototype aromatic molecule, $C_5H_5^-$.

Stability is an important feature of aromatic compounds. We performed an *ab initio mol*ecular dynamics (Atom−centered Density Matrix Propagation (ADMP)[25] simulation) at 298 K and at 400 K temperatures for 1000 fs timescale on $X_2Y_3^-$ and $X_3Y_2^-$ molecules. All the structures remain intact during the simulation at both the temperatures, indicating their kinetic stability. The energy value fluctuates regularly with the increase in the thermal kinetic energy (see ESI†, Fig. S8). The fluctuations are greater for 400 K than for 298 K because of the increased nuclear kinetic energy.
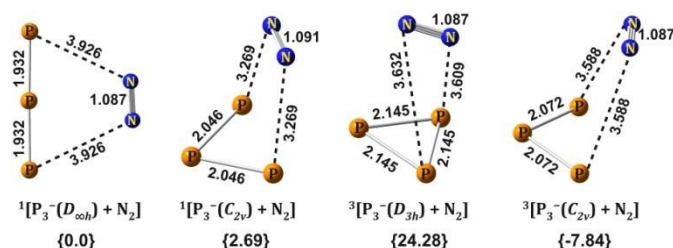


**Fig. 7** Four different minima of $P_3^-$ with $N_2$. Symmetry of $P_3^-$ is shown in the parenthesis. Distances are in Å units. Relative free energies (in kcal/mol) are shown in braces.

To examine the feasibility of synthetic realization of the proposed molecules, we propose a potential synthetic route for the formation of $P_3N_2^-$ – a click reaction between $P_3^-$ and $N_2$. $P_3^-$ is experimentally known[37a] and theoretically characterized as well.[37b] $P_3^-$ is proposed to have a number of nearly isoenergy minima, such as linear ($^1D_{\infty h}$), bent ($^{1,3}C_{2v}$) and equilateraral triangle ($^3D_{3h}$ symmetry) (see ESI†,

**4** | *Phys. Chem. Chem. Phys.*, 2015, **00**, 1-8

This journal is © The Royal Society of Chemistry 20xx

Table S9). A dispersion complex between $P_3^-$ and $N_2$ is optimized first, in which the symmetry in $P_3^-$ unit is retained (Fig. 7). The singlet and triplet surfaces are generated by interpolating between the geometries of the reactant and the product of similar spin state, and evaluation single point energy. Although $^3D_{3h}$ species is the least energy structure of $P_3^-$, we have considered only the singlet state species as the plausible reactants, because the triplet state of the product ($P_3N_2^-$) is high in energy ($\Delta G_{298} = 50.77$ kcal/mol) compared to the product in singlet state (see Fig. 8).
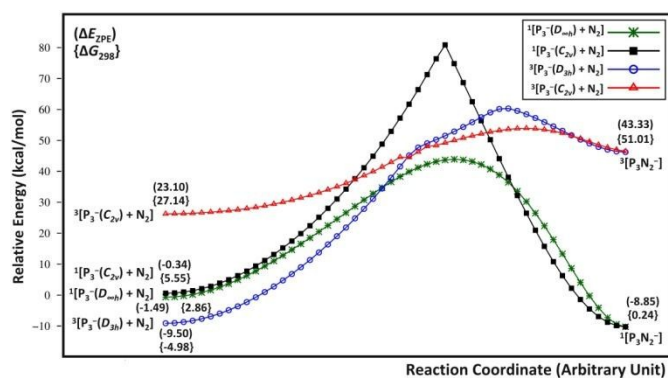


**Fig. 8** The singlet and triplet surfaces for the plausible production of $P_3N_2^-$; green and black surfaces are for singlet states and red and blue surfaces are for triplet states.

Both the singlet state minima of $P_3^-$ (*viz.* $^1D_{\infty h}$ and $^1C_{2v}$) are considered for the plausible click reaction with $N_2$. We found that only the singlet linear ($^1D_{\infty h}$) $P_3^-$ is reacting with $N_2$ through a single step concerted mechanism. The transition state (TS) corresponds to a synchronous addition of terminal P−N bonds with P−N distances of 2.361 Å and have $C_{2v}$ symmetry. The free energy of activation ($\Delta^{\ddagger}G_{298}$) for the formation of $P_3N_2^-$ (from $P_3^-$ and $N_2$) is 30.35 kcal/mol. This barrier is higher than the barrier for $P_2N_3^-$ formation from $P_2$ and $N_3^-$ (4.6 kcal/mol at the M06-2X/def2-TZVPPD level of theory).[11] The transition state is verified with the intrinsic reaction coordinate (IRC) calculations (see ESI†, Fig. S9). One of the reactants in the former reaction, $N_2$, is a highly stable molecule compared to the reactants in the latter reaction, azide ion ($N_3^-$) and $P_2$. This contributes to the higher activation energy for the formation of $P_3N_2^-$. The reaction is exothermic ($\Delta_r H_{298} = -9.22$ kcal/mol) and exergonic ($\Delta_r G_{298} = -2.61$ kcal/mol). Reverse process, retro-click reaction, has high barrier ($\Delta^{\ddagger}G_{298} = 39.57$ kcal/mol) which indicates that $P_3N_2^-$ is stable towards a potential dissociation pathway.
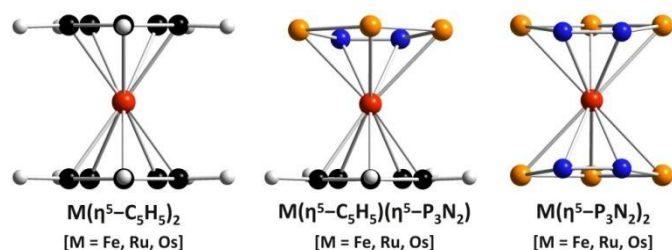


**Fig. 9** Optimized geometries of metallocenes.

We explored the possibility of using $P_3N_2^-$ as a $\eta^5$-ligand in metallocenes. Scherer *et al.* have shown that $P_5^-$ can substitute a $C_5Me_5^-$ group from decamethylmetallocenes, $M(\eta^5\text{-}C_5Me_5)_2$, (M=Fe,

Ru).[8d] We have studied the metallocenes (M=Fe, Ru, Os) with $P_3N_2^-$ as one of the $\eta^5$-ligands. The complex formation from the fragments is favorable with large negative enthalpy of formation ($\Delta H_f$) and free energy of formation ($\Delta G_f$) and large positive dissociation energies (Table 3). We have also included the solvation effect for calculating the dissociation energy. Polarizable Continuum Model (PCM) with benzene as a solvent ($\varepsilon = 2.27$) was used because the preparation of ferrocene is done in anhydrous benzene. Large negative values of formation energy ($\Delta E_f^{sol}$) even after the inclusion of solvation effect ensure the viability of $P_3N_2^-$ substituted metallocenes.

**Table 3** Zero point energy corrected dissociation energy ($D_o^{ZPE}$) for the dissociation of metal complex to its fragments (e.g., $Fe(\eta^5\text{-}C_5H_5)_2 \to Fe^{+2} + 2\,C_5H_5^-$), the enthalpy of formation ($\Delta H_f$), the free energy of formation ($\Delta G_f$) and the formation energy with solvation effect ($\Delta E_f^{sol}$, solvent: benzene; $\varepsilon = 2.27$) for the formation of metal complex from fragments (e.g., $Fe^{+2} + 2\,C_5H_5^- \to Fe(\eta^5\text{-}C_5H_5)_2$) at the M06-L/def2-TZVP level of theory. All energies are shown in kcal/mol.

| System | $D_0^{ZPE}$ | $\Delta H_f$ | $\Delta G_f$ | $\Delta E_f^{sol}$ |
|---|---|---|---|---|
| $Fe(\eta^5\text{-}C_5H_5)_2$ | 748.43 | -750.40 | -729.20 | -459.43 |
| $Fe(\eta^5\text{-}C_5H_5)(\eta^5\text{-}P_3N_2)$ | 712.84 | -714.31 | -692.54 | -426.94 |
| $Fe(\eta^5\text{-}C_5Me_5)(\eta^5\text{-}P_3N_2)$ | 729.21 | -730.11 | -706.14 | -451.44 |
| $Fe(\eta^5\text{-}P_3N_2)_2$ | 661.66 | -662.52 | -640.27 | -376.83 |
| $Ru(\eta^5\text{-}C_5H_5)_2$ | 770.54 | -772.22 | -751.55 | -481.44 |
| $Ru(\eta^5\text{-}C_5H_5)(\eta^5\text{-}P_3N_2)$ | 738.94 | -740.13 | -718.65 | -453.15 |
| $Ru(\eta^5\text{-}C_5Me_5)(\eta^5\text{-}P_3N_2)$ | 754.46 | -754.73 | -732.54 | -476.25 |
| $Ru(\eta^5\text{-}P_3N_2)_2$ | 692.49 | -693.12 | -671.13 | -407.65 |
| $Os(\eta^5\text{-}C_5H_5)_2$ | 850.55 | -852.45 | -830.96 | -572.53 |
| $Os(\eta^5\text{-}C_5H_5)(\eta^5\text{-}P_3N_2)$ | 817.48 | -818.84 | -796.53 | -542.64 |
| $Os(\eta^5\text{-}C_5Me_5)(\eta^5\text{-}P_3N_2)$ | 832.85 | -833.36 | -809.61 | -565.55 |
| $Os(\eta^5\text{-}P_3N_2)_2$ | 768.93 | -769.65 | -747.02 | -494.87 |

The $P_3N_2^-$ ring in $M[(\eta^5\text{-}C_5H_5)(\eta^5\text{-}P_3N_2)]$, [M=Fe, Ru, Os], is tilted (Fig. 9), with shorter Fe-N distances than Fe-P distances due to different atomic sizes of P and N atoms. As per NBO analysis, bonding between the Fe atom and the atoms of $P_3N_2$ moiety is covalent. HOMO of the $Fe[(\eta^5\text{-}C_5Me_5)(\eta^5\text{-}P_3N_2)]$ have the interaction of $d_z^2$ orbital of the Fe atom and the delocalized $\pi$-orbital of $P_3N_2$ unit. Interaction energies from energy decomposition analysis (EDA)[29] are negative (stabilizing interactions), with 99% of attractive contribution from electrostatic ($\Delta E_{elstat}$) and orbital ($\Delta E_{orb}$) terms (Table 4). In all the cases the $\Delta E_{elstat}$ is slightly larger than the $\Delta E_{orb}$ term, while the $\Delta E_{orb}$ is very small compared to the previous two terms. Therefore the interaction is mostly electrostatic type, which is expected as the two anionic aromatic rings are electrostatically attached to the $M^{2+}$. In $M(\eta^5\text{-}C_5H_5)_2$ the $\Delta E_{elstat}$ term is quite large (*ca.* 57-58%) than the $\Delta E_{orb}$ term (*ca.* 41-42%); while the $\Delta E_{elstat}$ term is significantly reduced on introducing $P_3N_2$ units. In case of $M(\eta^5\text{-}C_5H_5)_2$ the $\Delta E_{elstat}$ term (*ca.* 51-53%) and $\Delta E_{orb}$ term (*ca.* 46-48%) becomes of nearly equal weightage. The increase in the $\Delta E_{orb}$ term in $P_3N_2$ complex (*ca.* 5-6%) indicates better bonding than that in $C_5H_5^-$ complex.

This journal is © The Royal Society of Chemistry 20xx

*Phys. Chem. Chem. Phys.*, 2015, **00**, 1-8 | **5**

**Table 4** Energy decomposition analysis results of the metallocenes. All the energy values are in kcal/mol. The total interaction energy ($\Delta E_{int}$) is calculated as a sum of Pauli repulsion energy ($\Delta E_{Pauli}$), electrostatic attraction energy ($\Delta E_{elstat}$), energy due to orbital contribution ($\Delta E_{orb}$) and the dispersion energy ($\Delta E_{disp}$) terms. The percentage contribution towards the total attractive interaction ($\Delta E_{elstat} + \Delta E_{orb} + \Delta E_{disp}$) is shown in parenthesis.

| Molecules | Fragments | $\Delta E_{int}$ | $\Delta E_{Pauli}$ | $\Delta E_{elstat}$ | $\Delta E_{orb}$ | $\Delta E_{disp}$ |
|---|---|---|---|---|---|---|
| $Fe(\eta^5-C_5H_5)_2$ | $[Fe(\eta^5-C_5H_5)]^+ + C_5H_5^-$ | -245.13 | 206.72 | -257.67 (57.03%) | -190.18 (42.09%) | -4.00 (0.88%) |
| $Fe(\eta^5-C_5H_5)(\eta^5-P_3N_2)$ | $[Fe(\eta^5-C_5H_5)]^+ + P_3N_2^-$ | -208.96 | 200.43 | -208.97 (51.04%) | -197.06 (48.14%) | -3.36 (0.82%) |
| $Fe(\eta^5-C_5Me_5)(\eta^5-P_3N_2)$ | $[Fe(\eta^5-C_5Me_5)]^+ + P_3N_2^-$ | -195.95 | 215.43 | -213.76 (51.96%) | -191.67 (46.59%) | -5.95 (1.45%) |
| $Fe(\eta^5-P_3N_2)_2$ | $[Fe(\eta^5-P_3N_2)]^+ + P_3N_2^-$ | -205.79 | 240.25 | -227.92 (51.10%) | -214.68 (48.13%) | -3.44 (0.77%) |
| $Ru(\eta^5-C_5H_5)_2$ | $[Ru(\eta^5-C_5H_5)]^+ + C_5H_5^-$ | -232.75 | 232.70 | -270.99 (58.22%) | -191.82 (41.21%) | -2.64 (0.57%) |
| $Ru(\eta^5-C_5H_5)(\eta^5-P_3N_2)$ | $[Ru(\eta^5-C_5H_5)]^+ + P_3N_2^-$ | -201.29 | 243.57 | -234.63 (52.74%) | -207.21 (46.58%) | -3.02 (0.68%) |
| $Ru(\eta^5-C_5Me_5)(\eta^5-P_3N_2)$ | $[Ru(\eta^5-C_5Me_5)]^+ + P_3N_2^-$ | -183.15 | 247.07 | -232.86 (54.13%) | -192.44 (44.73%) | -4.92 (1.14%) |
| $Ru(\eta^5-P_3N_2)_2$ | $[Ru(\eta^5-P_3N_2)]^+ + P_3N_2^-$ | -206.19 | 244.27 | -235.18 (52.21%) | -212.03 (47.07%) | -3.25 (0.72%) |
| $Os(\eta^5-C_5H_5)_2$ | $[Os(\eta^5-C_5H_5)]^+ + C_5H_5^-$ | -252.21 | 319.43 | -333.13 (58.28%) | -235.04 (41.12%) | -3.47 (0.60%) |
| $Os(\eta^5-C_5H_5)(\eta^5-P_3N_2)$ | $[Os(\eta^5-C_5H_5)]^+ + P_3N_2^-$ | -221.24 | 332.26 | -291.66 (52.69%) | -258.80 (46.76%) | -3.04 (0.55%) |
| $Os(\eta^5-C_5Me_5)(\eta^5-P_3N_2)$ | $[Os(\eta^5-C_5Me_5)]^+ + P_3N_2^-$ | -204.23 | 343.58 | -294.04 (53.68%) | -248.74 (45.41%) | -5.03 (0.91%) |
| $Os(\eta^5-P_3N_2)_2$ | $[Os(\eta^5-P_3N_2)]^+ + P_3N_2^-$ | -219.43 | 345.77 | -298.59 (52.83%) | -263.23 (46.57%) | -3.38 (0.60%) |

## Conclusions

The electronic properties of a novel cyclic all-pnictogen five membered ring, $P_3N_2^-$, bearing 6π electrons, was analyzed using quantum chemical methods. The optimized singlet ground state has a planar $C_{2v}$ symmetric geometry. All the bonds are covalent with bond orders in between 1 and 2. The negative charge is delocalized over the framework. The aromaticity of this molecule was characterized with various NICS based approaches. The existence of a circulating diatropic ring current over the molecular frame further supports the aromatic nature. Reaction profile for a plausible synthetic route to $P_3N_2^-$ was calculated – a cycloaddition between linear $P_3^-$ ion and $N_2$ through a concerted $C_{2v}$ symmetric transition state. Free energy of reaction implies the formation to be spontaneous. The heavier analogues of this molecule ($X_3Y_2^-$) as well as the closely related molecules ($X_2Y_3^-$) are also found to be aromatic in terms of all the criteria we have employed here. All these structures are kinetically stable as shown by *ab initio* molecular dynamics study. Thus $P_3N_2^-$, and heavier all-pnictogen pentacyclic anions are potential candidates for synthetic realization.

## Acknowledgements

## Notes and references

1  A. Kekulé, *Justus Liebigs Ann. Chem.*, 1866, **137**, 129–196.
2  (a) P. v. R. Schleyer and H. Jiao, *Pure Appl. Chem.*, 1996, **68**, 209–218; (b) P. v. R. Schleyer, C. Maerker, A. Dransfeld, H. Jiao and N. J. R. v. E. Hommes, *J. Am. Chem. Soc.*, 1996, **118**, 6317–6318; (c) J. Kruszewski and T. M. Krygowski, *Tetrahedron Lett.*, 1972, **13**, 3839–3842; (d) J. A. N. F. Gomes and R. B. Mallion, *Chem. Rev.*, 2001, **101**, 1349–1384; (e) G. Merino, T. Heine and G. Seifert, *Chem. Eur. J.*, 2004, **10**, 4367–4371; (f) *Aromaticity and Metal Clusters*, ed. P. K. Chattaraj, CRC Press, Taylor & Francis Group, Boca Raton, FL, 2011; (g) P. v. R. Schleyer, P. Freeman, H. Jiao and B. Goldfuss, *Angew. Chem. Int. Ed. Engl.*, 1995, **34**, 337–340; (h) S. Pan, R. Saha, S. Mandal and P. K. Chattaraj, *Phys. Chem. Chem. Phys.*, 2015, DOI: 10.1039/C5CP06282A.
3  (a) X. Li, A. E. Kuznetsov, H.–F. Zhang, A. I. Boldyrev and L.–S. Wang, *Science*, 2001, **291**, 859–861; (b) A. I. Boldyrev and L.–S. Wang, *Chem. Rev.*, 2005, **105**, 3716–3757.
4  (a) G. He, O. Shynkaruk, M. W. Lui and E. Rivard, *Chem. Rev.*, 2014, **114**, 7815–7880; (b) M. S. Balakrishna, D. J. Eislera and T. Chivers, *Chem. Soc. Rev.*, 2007, **36**, 650–664; (c) M. W. Schmidt, M. S. Gordon and J. A. Boatz, *Int. J. Quantum Chem.*, 2000, **76**, 434–446; (d) M. N. Glukhovtsev, H. Jiao and P. v. R. Schleyer, *Inorg. Chem.*, 1996, **35**, 7124–7133.
5  (a) A. Vij, J. G. Pavlovich, W. W. Wilson, V. Vij and K. O. Christe, *Angew. Chem. Int. Ed.*, 2002, **41**, 3051–3054; (b) M.-T. Nguyen,

M. Sana, G. Leroy and J. Elguero, *Can. J. Chem.*, 1983, **61**, 1435–1439; (c) M. T. Nguyen, M. A. McGinn, A. F. Hegarty and Elguéro, *Polyhedron*, 1985, **4**, 1721–1726.

6 (a) K. O. Christe, W. W. Wilson, J. A. Sheehy and J. A. Boatz, *Angew. Chem. Int. Ed.*, 1999, **38**, 2004–2009; (b) A. Vij, W. W. Wilson, V. Vij, F. S. Tham, J. A. Sheehy and K. O. Christe, *J. Am. Chem. Soc.*, 2001, **123**, 6308–6313.

7 (a) A. Vogler, R. E. Wright and H. Kunkely, *Angew. Chem. Int. Ed. Engl.*, 1980, **19**, 717–718; (b) H. Huber, *Angew. Chem. Int. Ed. Engl.*, 1982, **21**, 64–65; (c) P. Saxe, and H. F. Schaefer, *J. Am. Chem. Soc.*, 1983, **105**, 1760–1764; (d) R. Engelke, *J. Phys. Chem.*, 1989, **93**, 5722–5727.

8 (a) M. Baudler, S. Akpapoglou, D. Ouzounis, F. Wasgestian, B. Meinigke, H. Budzikiewicz and H. Münster, *Angew. Chem. Int. Ed. Engl.*, 1988, **27**, 280–281; (b) E. J. P. Malar, *J. Org. Chem.*, 1992, **57**, 3694–3698; (c) M. N. Glukhovtsev, P. v. R. Schleyer and C. Maerker, *J. Phys. Chem.*, 1993, **97**, 8200–8206; (d) O. J. Scherer, T. Brück and G. Wolmershäuser, *Chem. Ber.*, 1988, **121**, 935–938.

9 (a) T. R. Galeev and A. I. Boldyrev, *Phys. Chem. Chem. Phys.*, 2011, **13**, 20549–20556; (b) D. S. Warren and B. M. Gimarc, *J. Am. Chem. Soc.*, 1992, **114**, 5378–5385.

10 (a) T. J. Millar, A. Bennett and E. Herbst, *Mon. Not. R. astr. Soc.*, 1987, **229**, 41p–44p; (b) R. Atkins and P. L. Timms, *Spectrochim. Acta*, 1977, **33**, 853–857; (c) G. M. Chaban, N. M. Klimenko and O. P. Charkin, *Bull. Acad. Sci. U.S.S.R.*, 1990, **39**, 1440–1446; (d) R. Ahlrichs, M. Bär, H. S. Plitt and H. Schnöckel, *Chem. Phys. Lett.*, 1989, **161**, 179–184.

11 A. Velian and C. C. Cummins, *Science*, 2015, **348**, 1001–1004.

12 M. J. Frisch, G. W. Trucks, H. B. Schlegel, G. E. Scuseria, M. A. Robb, J. R. Cheeseman, G. Scalmani, V. Barone, B. Mennucci, G. A. Petersson, H. Nakatsuji, M. Caricato, X. Li, H. P. Hratchian, A. F. Izmaylov, J. Bloino, G. Zheng, J. L. Sonnenberg, M. Hada, M. Ehara, K. Toyota, R. Fukuda, J. Hasegawa, M. Ishida, T. Nakajima, Y. Honda, O. Kitao, H. Nakai, T. Vreven, J. A. Montgomery, Jr., J. E. Peralta, F. Ogliaro, M. Bearpark, J. J. Heyd, E. Brothers, K. N. Kudin, V. N. Staroverov, R. Kobayashi, J. Normand, K. Raghavachari, A. Rendell, J. C. Burant, S. S. Iyengar, J. Tomasi, M. Cossi, N. Rega, J. M. Millam, M. Klene, J. E. Knox, J. B. Cross, V. Bakken, C. Adamo, J. Jaramillo, R. Gomperts, R. E. Stratmann, O. Yazyev, A. J. Austin, R. Cammi, C. Pomelli, J. W. Ochterski, R. L. Martin, K. Morokuma, V. G. Zakrzewski, G. A. Voth, P. Salvador, J. J. Dannenberg, S. Dapprich, A. D. Daniels, Ö. Farkas, J. B. Foresman, J. V. Ortiz, J. Cioslowski and D. J. Fox, *Gaussian 09 (Revision C.01)*, Gaussian, Inc., Wallingford, CT, 2010.

13 Y. Zhao and D. G. Truhlar, *Theor. Chem. Acc.*, 2008, **120**, 215–241.

14 D. Rappoport and F. Furche, *J. Chem. Phys.*, 2010, **133**, 134105.

15 B. Metz, H. Stoll and M. Dolg, *J. Chem. Phys.*, 2000, **113**, 2563.

16 (a) *Atoms in Molecules: A Quantum Theory, ed. R. F. W. Bader, Oxford University Press, Oxford, 1990; (b)* D. Cremer and E. Kraka, *Angew. Chem. Int. Ed. Engl.*, 1984, **23**, 627–628; (c) P. Macchi, D. M. Proserpio and A. Sironi, *J. Am. Chem. Soc.*, 1998, **120**, 13429–13435; (d) P. Macchi, L. Garlaschelli, S. Martinengo and A. Sironi, *J. Am. Chem. Soc.*, 1999, **121**, 10428–10429.

17 T. Lu and F. W. Chen, *J. Comput. Chem.*, 2012, **33**, 580–592.

18 (a) S. Huzinaga and B. Miguel, *Chem. Phys. Lett.*, 1990, **175**, 289–291; (b) S. Huzinaga and M. Klobukowski, *Chem. Phys. Lett.*, 1993, **212**, 260–264; (c) S. Pan, A. Gupta, S. Mandal, D. Moreno, G. Merino and P. K. Chattaraj, *Phys. Chem. Chem. Phys.*, 2015, **17**, 972–982.

19 (a) J. P. Foster and F. Weinhold, *J. Am. Chem. Soc.*, 1980, **102**, 7211–7218; (b) E. D. Glendening and F. Weinhold, *J. Comp. Chem.*, 1998, **19**, 593–609; (c) A. E. Reed, R. B. Weinstock and F. Weinhold, *J. Chem. Phys.*, 1985, **83**, 735–746.

20 E. D. Glendening, J. K. Badenhoop, A. E. Reed, J. E. Carpenter, J. A. Bohmann, C. M. Morales and F. Weinhold, *NBO 5.9.*, Theoretical Chemistry Institute, University of Wisconsin, Madison, WI, 2012.

21 K. B. Wiberg, *Tetrahedron*, 1968, **24**, 1083–1096.

22 T. A. Keith, *AIMAll (Version 15.05.18)*, TK Gristmill Software, Overland Park KS, USA, 2015.

23 (a) K. Eichkorn, F. Weigend, O. Treutler and R. Ahlrichs, *Theor. Chem. Acc.*, 1997, **97**, 119–124; (b) F. Weigend and R. Ahlrichs, *Phys. Chem. Chem. Phys.*, 2005, **7**, 3297–3305.

24 (a) K. Wolinski, J. F. Hilton and P. Pulay, *J. Am. Chem. Soc.*, 1990, **112**, 8251–8260; (b) J. R. Cheeseman, G. W. Trucks, T. A. Keith and M. J. Frisch, *J. Chem. Phys.*, 1996, **104**, 5497–5509.

25 (a) H. B. Schlegel, J. M. Millam, S. S. Iyengar, G. A. Voth, G. E. Scuseria, A. D. Daniels and M. J. Frisch, *J. Chem. Phys.*, 2001, **114**, 9758-9763; (b) S. S. Iyengar, H. B. Schlegel, J. M. Millam, G. A. Voth, G. E. Scuseria and M. J. Frisch, *J. Chem. Phys.*, 2001, **115**, 10291-10302.

26 F. Weigend, M. Häser, H. Patzelt and R. Ahlrich, *Chem. Phys. Lett.*, 1998, **294**, 143–152.

27 Y. Zhao and D. G. Truhlar, *J. Chem. Phys.*, 2006, **125**, 194101.

28 P. J. Hay and W. R. Wadt, *J. Chem. Phys.*, 1985, **82**, 270–283.

29 (a) K. Morokuma, *Acc. Chem. Res.*, 1977, **10**, 294–300; (b) T. Ziegler and A. Rauk, *Theor. Chim. Acta*, 1977, **46**, 1–10; (c) T. Ziegler, A. Rauk and E. J. Baerends, *Theor. Chim. Acta*, 1977, **43**, 261–271.

30 G. t. Velde, F. M. Bickelhaupt, E. J. Baerends, C. F. Guerra, S. J. A. v. Gisbergen, J. G. Snijders, and T. Ziegler, *J. Comput. Chem.*, 2001, **22**, 931–967.

31 (a) E. A. Carter and W. A. Goddard III, *J. Phys. Chem.*, 1986, **90**, 998–1001; (b) R. G. Pearson, *J. Org. Chem.*, 1989, **54**, 1423–

This journal is © The Royal Society of Chemistry 20xx

*Phys. Chem. Chem. Phys.*, 2015, **00**, 1-8 | **7**

1430; (c) Z. Zhou and R. G. Parr, *J. Am. Chem. Soc.*, 1990, **112**, 5720–5724.

32 a) R. G. Parr and P. K. Chattaraj, *J. Am. Chem. Soc.*, 1991, **113**, 1854–1855; (b) R. G. Pearson, *Acc. Chem. Res.*, 1993, **26**, 250–255.

33 (a) P. Pyykkö and M. Atsumi, *Chem. Eur. J.*, 2009, **15**, 186–197; (b) P. Pyykkö and M. Atsumi, *Chem. Eur. J.*, 2009, **15**, 12770–12779.

34 (a) C. Corminboeuf, T. Heine, G. Seifert, P. v. R. Schleyer, J. Weber, *Phys. Chem. Chem. Phys.*, 2004, **6**, 273–276; (b) J. J. Torres-Vega, A. Vásquez-Espinal, J. Caballero, M. L. Valenzuela, L. Alvarez-Thon, E. Osorio and W. Tiznado, *Inorg. Chem.*, 2014, **53**, 3579–3585; (c) S. Noorizadeh and M. Dardab, *Chem. Phys. Lett.*, 2010, **493**, 376–380.

35 (a) E. Steiner and P. W. Fowler, *Int. J. Quantum Chem.*, 1996, **60**, 609–616; (b) P. W. Fowler and E. Steiner, *J. Phys. Chem. A*, 1997, **101**, 1409–1413; (c) R. W. A. Havenith, J. J. Engelberts, P. W. Fowler, E. Steiner, J. H. v. Lentheb and P. Lazzeretti, *Phys. Chem. Chem. Phys.*, 2004, **6**, 289–294.

36 (a) E. Steiner and P. W. Fowler, *Chem. Commun.*, 2001, 2220–2221; (b) E. Steiner and P. W. Fowler, *Org. Biomol. Chem.*, 2004, **2**, 34–37.

37 (a) R. O. Jones, G. Ganteför, S. Hunsicker and P. Pieperhoff, *J. Chem. Phys.*, 1995, **103**, 9549–9562; (b) T. P. Hamilton and H. F. Schaefer III, *Chem. Phys. Lett.*, 1990, **166**, 303–306.